

## Zirconium doped $\text{LiNi}_{0.91}\text{Co}_{0.06}\text{Mn}_{0.03}\text{O}_2$ cathode as a superior cathode for lithium ion batteries

Seung-Hwan Lee\*

Department of Advanced Materials Engineering, Daejeon University, Daejeon 34520, Republic of Korea

In this paper, well-crystallized Zr-doped Ni-rich layered  $\text{LiNi}_{0.91}\text{Co}_{0.06}\text{Mn}_{0.03}\text{O}_2$  cathode is prepared by solid state method and its structural properties and electrochemical performances in lithium-ion cells is investigated. The Zr-doped  $\text{LiNi}_{0.91}\text{Co}_{0.06}\text{Mn}_{0.03}\text{O}_2$  has superior cation ordering and the morphology of Zr-doped  $\text{LiNi}_{0.91}\text{Co}_{0.06}\text{Mn}_{0.03}\text{O}_2$  was the same as pristine  $\text{LiNi}_{0.91}\text{Co}_{0.06}\text{Mn}_{0.03}\text{O}_2$ . The 0.5 wt% Zr-doped  $\text{LiNi}_{0.91}\text{Co}_{0.06}\text{Mn}_{0.03}\text{O}_2$  shows better electrochemical performances such as initial discharge capacity of  $210.5 \text{ mAh g}^{-1}$ , rate capability of 75.4 % at 2 C and cycling retention of 94.5 % after 50 cycles. It can be elucidated by the role of the  $\text{Li}_2\text{ZrO}_3$  layer and Zr substitution in  $\text{LiNi}_{0.91}\text{Co}_{0.06}\text{Mn}_{0.03}\text{O}_2$ .

**Keywords:** Zr-doped Ni-rich layered  $\text{LiNi}_{0.91}\text{Co}_{0.06}\text{Mn}_{0.03}\text{O}_2$ , Cation ordering, Morphology, Electrochemical performances.

### Introduction

Nowadays, lithium ion batteries (LIBs) have received attention as an outstanding main power source to meet the high energy density for electric vehicles (EVs) and portable devices. It is well known that cathode is the key component, determining the battery performance [1, 2]. Among many cathodes, the Ni-rich  $\text{LiNi}_x\text{Co}_y\text{Mn}_z\text{O}_2$  (NCM,  $x \geq 0.8$ ,  $x + y + z = 1$ ) materials have stood out as the promising candidate due to its smaller volume change ( $\text{LiCoO}_2$ ), superior specific capacity ( $\text{LiNiO}_2$ ) and excellent thermal stability ( $\text{LiMn}_2\text{O}_4$ ) [3]. Unfortunately, Ni-rich NCM cathodes still suffer from inferior long-term cycling performance, especially, it is proportional to the Ni content. It can be explained by unwanted side reaction at the interface between cathode and electrolyte. It leads to phase transformation from layered to disordered spinel/rock-salt, the reduction of  $\text{Ni}^{4+}$  and oxygen loss, resulting in severe structural degradation [4]. This phenomenon causes the rapid increase of cathode impedance and capacity decay of Ni-rich NCM during cycling [5].

Many approaches such as coating [6], doping [7] and single crystal [8] have been studied to enhance the electrochemical performance of Ni-rich NCM. Among them, a lot of doping effects have been reported to increase cycle life of Ni-rich cathodes [9-11]. This is because the dopant ion can reduce the cation mixing, stabilizing the crystal structure from volume changes during cycling. Among various dopants, the Zr-doped NCM cathode showed excellent electrochemical per-

formance. However, as far as we know, there have been no reports of NCM cathodes with a Ni content of 91%.

In this paper, we synthesize the Zr-doped Ni-rich  $\text{LiNi}_{0.91}\text{Co}_{0.06}\text{Mn}_{0.03}\text{O}_2$  (NCM91) with high crystallinity and investigate the effect of doping to improve the structural stability and electrochemical performances. These results indicate that suitable amount of Zr substitution delivers the superior electrochemical performances.

### Experimental

$\text{Ni}_{0.91}\text{Co}_{0.06}\text{Mn}_{0.03}(\text{OH})_2$  precursor was prepared by using aqueous solution of  $\text{NiSO}_4 \cdot 6\text{H}_2\text{O}$ ,  $\text{CoSO}_4 \cdot 7\text{H}_2\text{O}$  and  $\text{MnSO}_4 \cdot \text{H}_2\text{O}$  via a co-precipitation method. A NaOH and  $\text{NH}_4\text{OH}$  solution as a chelating agent were used. The as-prepared  $\text{Ni}_{0.91}\text{Co}_{0.06}\text{Mn}_{0.03}(\text{OH})_2$  precursor was mixed with  $\text{LiOH} \cdot \text{H}_2\text{O}$  at a molar ratio of 1 : 1.05 and 0.5 wt%  $\text{ZrO}_2$  as a zirconium source in a molar ratio of 1.0 wt%. Afterward, the mixed powders were sintered at 500 °C for 5 h and 680 °C for 15 h in air for pristine and Zr-doped NCM91.

The structural properties of the pristine and Zr-doped NCM91 were conducted by X-ray diffraction (XRD, X-pert PRO MPD, Philips, Cu  $K\alpha$ ) and field emission scanning electron microscopy (FESEM, S-4800, HITACHI) equipped with an energy dispersive X-ray detector (EDX, X-maxN, HORIBA).

All electrochemical performances were evaluated based on a 2032 coin cells. The pristine and Zr-doped NCM91 cathodes were prepared by mixing active materials, super P black (conductive material) and polyvinylidene fluoride (PVDF, binder) with a weight ratio of 96 : 2 : 2. After that, the mixed slurry was coated on Al foil (16  $\mu\text{m}$  in thickness) and dried at 120

\*Corresponding author:  
Tel : +82-42-280-2414  
E-mail: shlee@dju.kr

$^{\circ}\text{C}$  for 12 h in a vacuum oven. The prepared cathode was punched with an electrode diameter of 14 mm and then dried at  $120^{\circ}\text{C}$  for 12 h in a vacuum oven. 1M  $\text{LiPF}_6$  in ethylene carbonate/ethylmethyl carbonate/dimethyl carbonate (1:1:1, v/v/v) was adopted as an electrolyte. Finally, coin cells were fabricated in an argon-filled glove box.

The electrochemical test was carried out galvanostatically in the voltage range of 3.0–4.3 V and various C-rates ( $1\text{C} = 210\text{ mAh g}^{-1}$ ) using electrochemical equipment (TOSCAT-3100, Toyo system) at room temperature.

## Results and Discussion

Fig. 1 shows the XRD patterns of pristine and Zr-doped NCM91. All the samples exhibited almost similar XRD patterns since small amount Zr doping does not significantly affect the NCM91 structure. All patterns indicate that synthesized samples belong to a layered hexagonal  $\alpha\text{-NaFeO}_2$  structure with the space

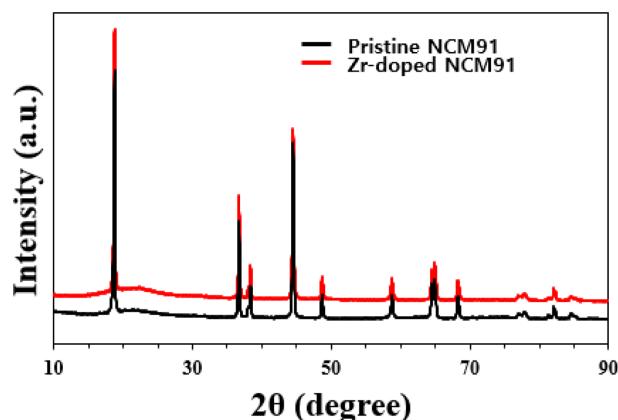


Fig. 1. XRD patterns of pristine and Zr doped NCM91.

group R-3m [2, 5]. The clear peak splitting of (006)/(102) and (108)/(110) indicates the well-developed hexagonal layered structure. However, for Zr-doped NCM91, there is a slight shift in the peak position to lower angles compared to the pristine NCM91. It can be explained by bigger ionic radius of Zr ( $0.72\text{ \AA}$ ) than that of  $\text{Ni}^{2+}$  ( $0.69\text{ \AA}$ ). Therefore it can be confirmed that Zr ions diffuse into the NCM91 structure. As listed in Table 1, the  $I_{(003)}/I_{(104)}$  ratios of the Zr-doped NCM91 are greater than that of pristine NCM91, indicating better structure stability and lower cation mixing of Zr-doped NCM91. It is believed that the Zr-doped NCM cathode can achieve high performances based on excellent structural stability.

Fig. 2 shows the FESEM images of the pristine and Zr-doped NCM91. All samples have similar spherical morphology with an average size of  $12\text{ }\mu\text{m}$ . Also, the spherical secondary particles are composed of small primary particles of approximately 200–500 nm. It can be seen that Zr doping not only does not change the spherical shape of NCM91, but also has little effect on the particle size. Moreover, the primary particles contacted each other directly. This can lower the resistance and improve the electrochemical performances. More importantly, we can see that the elements of Ni, Co, Mn and Zr were uniformly distributed, as shown in Fig. 3. We believe that the uniformly Zr-doped NCM91 can maximize the structural stability and electrochemical performances.

For electrochemical tests, the loading level of the NCM91 was adjusted about  $14.2\text{ mg/cm}^2$  because the high areal capacity is essential for practical application of LIBs [3]. Fig. 4 delivers the initial charge-discharge

Table 1.  $I_{(003)}/I_{(104)}$  ratios of pristine and Zr-doped NCM91

|                | $I_{(003)}/I_{(104)}$ |
|----------------|-----------------------|
| Pristine NCM91 | 1.25                  |
| Zr-doped NCM91 | 1.32                  |

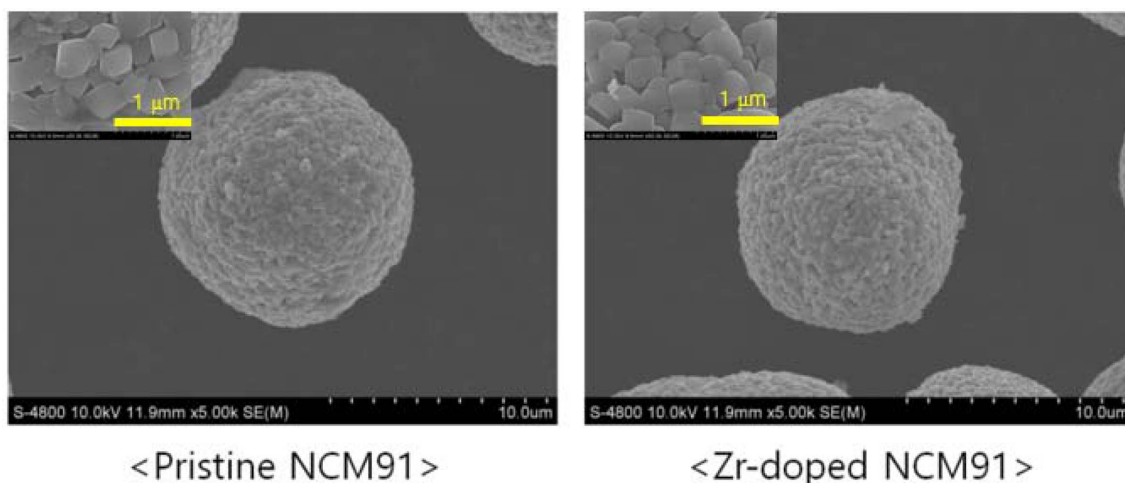


Fig. 2. FESEM images of the pristine and Zr-doped NCM91.

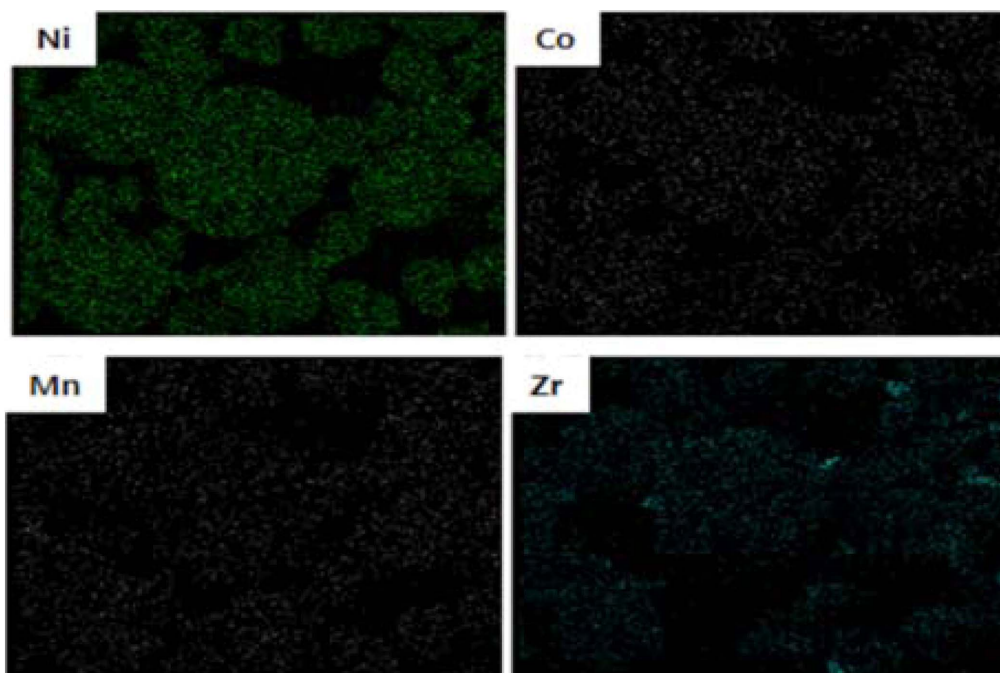


Fig. 3. EDS mapping of Zr-doped NCM91.

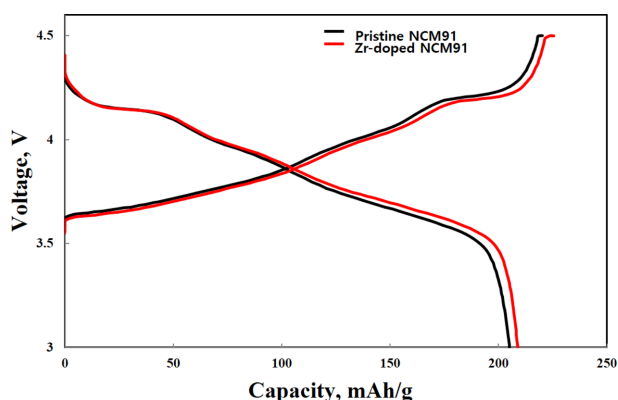


Fig. 4. Initial charge-discharge curves of pristine and Zr doped NCM91.

curves with pristine and different amount of Zr-doped NCM91 in a potential range of 3.0–4.3 V at 0.1 C. All samples have similar charge-discharge behaviors. It indicates that the Zr doping does not influence on electrochemical behaviors of the NCM91. The pristine NCM91 delivers the lower discharge capacity ( $216.8 \text{ mAh g}^{-1}$ ). However, Zr-doped NCM91 shows higher discharge curves ( $210.5 \text{ mAh g}^{-1}$ ), originated from the Zr incorporated into the crystal lattice. It can be explained by the enhanced conductivity of NCM91 compared to that of pristine NCM91 [5].

The rate capability of pristine and Zr-doped NCM91 at various C-rates from 0.1 C to 2 C are shown in Fig. 5. We can confirm that the capacity retention of all samples decreases as the C-rate increases. At low C-rates, all samples have almost the same capacity retention. However, as C-rate increased, the retention

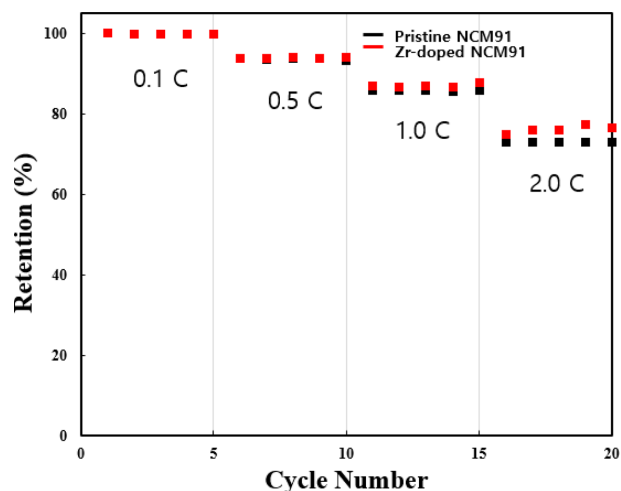
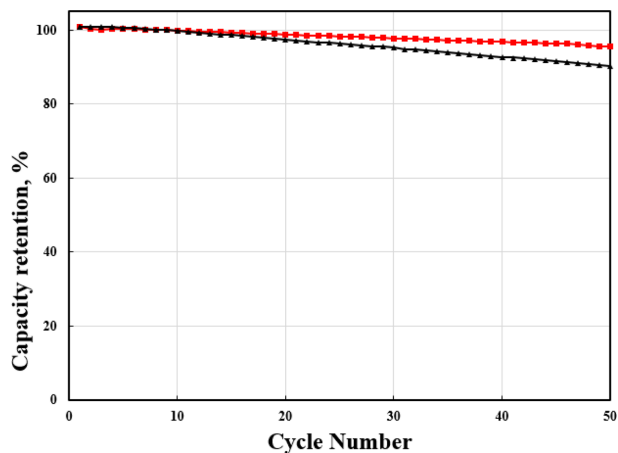


Fig. 5. Rate capability of pristine and Zr doped NCM91.

of pristine NCM91 sharply decreases, whereas Zr-doped NCM91 can suppress the retention decrease. It is closely related to the lower resistance of Zr-doped NCM91, resulting in fast Li ion kinetics [8].

Fig. 6 shows the cyclability of pristine and Zr-doped NCM91 at 0.5 C. The Zr-doped NCM91 show the superior cycle stability compared to pristine NCM. Especially, 0.5 wt% Zr-doped NCM91 shows the highest capacity retention after cycle test. The capacity retention of pristine NCM91 is 90.2% after 50 cycles. However, Zr-doped NCM display the 94.5% under the same condition. It is closely related to the contribution of Zr doping, resulting in reduction of charge transfer resistance of the electrolyte/NCM91 interface and alleviation of transition metal dissolution in NCM91 [4, 6, 9]. It can



**Fig. 6.** Cycle performance of pristine and Zr doped NCM91.

be inferred that Zr-doped NCM91 can maintain the excellent structural stability or surface chemistry with the electrolyte under long-term cycling. Yoon et al. reported that  $\text{Li}_2\text{ZrO}_3$  layer can be formed on the surface of cathode. The protective  $\text{Li}_2\text{ZrO}_3$  layer can be suppress the side reaction between electrolyte and NCM91 [12]. It is well known that the phase transition ( $\text{H2} \rightarrow \text{H3}$ ), which is one of the main reason for the capacity fading, by lattice shrinkage along the c-axis, leading to the volume change and micro-cracking [13]. Zr doping causes the phase stabilization of NCM91, enables the particles to maintain the original shape with accommodating the internal strain caused by the volume change [12].

## Conclusions

In this paper, we successfully synthesized pristine and Zr-doped NCM91 via solid-state reaction. Zr-doped NCM91 delivers superior structural properties as

well as electrochemical performances. The Zr-doped NCM91 with high crystallinity has smaller cation mixing compared to that of pristine NCM91 and maintain its original shape. The electrochemical performances of Zr-doped NCM91 outperforms pristine NCM91. This is because Zr doping not only reduces cation mixing, but also creates a synergistic effect by forming a  $\text{Li}_2\text{ZrO}_3$  protective layer on the NCM91 surface. Therefore, we can conclude that Zr doping into the NCM91 can be regarded as an one of the effective way for high performance NCM91 cathode.

## References

1. S.H. Lee, B.S. Jin, and H.S. Kim, *Sci. Rep.* 9 (2019) 17541.
2. J.W. Seok, J. Lee, T. Rodgers, D.H. Ko, and J.H. Shim, *Trans. Electr. Electron. Mater.* 20 (2019) 548–553.
3. S.H. Lee, H.S. Kim, and B.S. Jin, *J. Alloy. Comp.* 803 (2019) 1032-1036.
4. S.H. Lee, S. Lee, B.S. Jin, and H.S. Kim, *Sci. Rep.* 9 (2019) 8901.
5. J. Zhao, Z. Wang, J. Wang, H. Guo, X. Li, W. Gui, N. Chen, and D. Yan, *Energy Technology* 6 (2018) 2358-2366.
6. S.H. Lee, G.J. Park, S.J. Sim, B.S. Jin, and H.S. Kim, *J. Alloy. Comp.* 791 (2019) 193-199.
7. S.J. Sim, S.H. Lee, B.S. Jin, and H.S. Kim, *Sci. Rep.* 9 (2019) 8952.
8. S.H. Lee, S.J. Sim, B.S. Jin, and H.S. Kim, *Mater. Lett.* 270 (2020) 127615.
9. S.H. Lee, K.Y. Kim, and J.R. Yoon, *NPG Asia Materials* 12 (2020) 28.
10. Y. Lv, X. Cheng, W. Qiang, and B. Huang, *J. Power Sources* 450 (2020) 227718.
11. W. Yan, S. Yang, Y. Huang, Y. Yang, and G. Yuan, *J. Alloy. Comp.* 819 (2020) 153048.
12. S. Yoon, U.H. Kim, G.T. Park, S.J. Kim, K.H. Kim, J. Kim, and Y.K. Sun, *ACS Energy Lett.* 3 (2018) 1634-1639.
13. H.H. Sun and A. Manthiram, *Chem. Mater.* 29 (2017) 8486-8493.